Journal of Catalysis 256 (2008) 237–247

Contents lists available at ScienceDirect

Journal of Catalysis

www.elsevier.com/locate/jcat

Catalytic performance and characterization of Au/doped-ceria catalysts for the preferential CO oxidation reaction

G. Avgouropoulos [a,*], M. Manzoli [b], F. Boccuzzi [b], T. Tabakova [c], J. Papavasiliou [a], T. Ioannides [a], V. Idakiev [c]

[a] Foundation for Research and Technology-Hellas (FORTH), Institute of Chemical Engineering and High-Temperature Chemical Processes (ICE-HT), P.O. Box 1414, GR-26504 Patras, Greece
[b] Department of Chemistry IFM and NIS Centre of Excellence, University of Torino, via P. Giuria 7, 10125 Torino, Italy
[c] Institute of Catalysis, Bulgarian Academy of Sciences, Acad. G. Bonchev Str., Bl. 11, 1113 Sofia, Bulgaria

ARTICLE INFO

Article history:
Received 14 January 2008
Revised 17 March 2008
Accepted 17 March 2008
Available online 16 April 2008

Keywords:
Gold catalysts
Ceria
Deposition–precipitation
Hydrogen
Preferential CO oxidation
PROX
FTIR
HRTEM

ABSTRACT

The physicochemical properties and catalytic performance in the preferential CO oxidation (PROX) reaction of nanosized gold supported on doped-ceria were investigated. Zn- and Sm-doped Au/ceria catalysts were found to be more active than undoped Au/ceria, whereas the addition of lanthanum oxide had the opposite effect. A reductive pretreatment at 373 K for 1 h promoted catalytic activity. The ability of Au/doped ceria catalysts to tolerate the presence of CO_2 and H_2O in the feed was also studied. Adding CO_2 in the reactant feed provoked a decrease in catalyst activity; however, catalyst doping improved the resistance toward deactivation by CO_2. On the other hand, co-addition of CO_2 and H_2O counteracted the negative effect of CO_2, especially in the case of doped samples. IR studies of CO adsorbed at 90 K on the catalysts after different pretreatments gave information on the type of gold species present on the catalyst. The dispersion of gold depended on the nature of the dopant. Au/Zn–CeO_2 catalyst demonstrated the greatest dispersion as revealed by HRTEM measurements and comparison of FTIR intensity of the CO adsorption bands on the reduced samples. $AuCe_x$ clusters were formed on this catalyst by increasing the prereduction temperature. Large amounts of CO_2 were produced during the CO–O_2 interaction in the presence of a high concentration of zero-valent gold sites on the surface of the modified Au catalysts, confirming their important role in the CO oxidation reaction. IR spectra were collected after exposure to $CO + O_2 + H_2$ and also after addition of water in the PROX reaction mixture over Au/Zn–CeO_2 at 400 K. The evolution of the FTIR spectra run at 90 K after admission of O_2 on preadsorbed CO on the most active catalyst (i.e., Au/Zn–CeO_2) demonstrates the roles of the highly dispersed gold and the reduced support in activating oxygen.

1. Introduction

The development of efficient catalytic processes for the removal of carbon monoxide from hydrogen-rich gas mixtures has attracted worldwide research interest over the last decade due to its potential application in fuel cell energy systems. Solid polymer fuel cells (SPFCs), which typically operate at 353–373 K, appear to be a viable energy solution for automotive, portable, and stationary energy applications [1,2]. The chemical and physical properties of hydrogen, which is energy dense in mass but energy poor in volume, make the distribution and storage of pure hydrogen energy demanding. In addition, the lack of a worldwide infrastructure for transport and distribution of pure hydrogen (the ideal fuel for SPFCs), along with the presence of a well-established fossil fuel-based network, favors the near-term solution of onsite hydrogen production from hydrocarbons or alcohols (natural gas, methanol, ethanol) through steam or autothermal reforming and WGS reactions [1–6]. The gas mixture (i.e., reformate gas) produced by these processes contains 45–75 vol% H_2, 15–25 vol% CO_2, a few vol% H_2O, and 0.5–2 vol% CO. Optimum SPFC performance requires complete removal of carbon monoxide (to <10 ppm) from the hydrogen-rich gas stream, because CO, even in trace amounts, adsorbs strongly on currently used platinum anode electrocatalysts, thus inhibiting hydrogen adsorption and electrooxidation and significantly hampering cell performance [7,8]. Selective catalytic CO oxidation with molecular oxygen, also known as the preferential oxidation (PROX) reaction, is the simplest and most cost-effective method for removing CO from reformed fuels [3,9,10]. A high oxidation rate and high selectivity with respect to the undesired H_2 oxidation side reaction should characterize a candidate PROX catalyst. Moreover, PROX catalysts should be able to tolerate the high amounts of CO_2 and H_2O present in the reformate fuel.

The breakthrough research findings of Hutchings [11] and Haruta [12] demonstrated that highly dispersed gold nanoparticles supported on selected metal oxides can effectively oxidize CO with a very high reaction rate at much lower temperatures

* Corresponding author.
E-mail address: geoavg@iceht.forth.gr (G. Avgouropoulos).

0021-9517/$ – see front matter
doi:10.1016/j.jcat.2008.03.014

(even at subambient temperatures, i.e., 200 K) compared with conventional Pt-based catalysts. Numerous review articles have addressed the advances in the catalysis of gold over the last 20 years [13–20]. Recent results suggest that gold-based catalysts may be effectively used in the PROX reaction. This application is based on Haruta's demonstration that gold nanoparticles supported on reducible oxide supports are highly active for the CO oxidation reaction [12,21,22]. Three factors control the activity and the selectivity of gold catalysts and can affect their efficiency in the PROX reaction [13–20]: (a) size of the gold particles, (b) strong contact between the gold particles and the support, and (c) suitable selection of the support. Precipitation techniques are able to bring a strong interaction of gold nanoparticles (average gold particle size <3–5 nm) with the support. The strong interaction leads to the stabilization of small gold particles through a wider contact area and often gives the longest perimeter interface around them. The support plays an important role in the catalysis by gold, providing additional sites at the interface for the adsorption of the reactants close to the gold sites. Various reducible metal oxides, including Fe_2O_3, MnO_x, TiO_2, and CeO_2 [13–20], can play that role and also can supply oxygen to facilitate the oxidation of CO in the presence of H_2.

Comparative studies have shown that the support material can have a significant effect on the activity of gold catalysts in the PROX reaction [23–31]. The activity difference among the various catalysts is ascribed to the different sizes of gold clusters and the varying ability of the supports to supply oxygen to facilitate the CO oxidation reaction in the presence of H_2. CeO_2 is one of the most thermally stable compounds; under various redox conditions, the oxidation state of the cation may vary between +3 and +4. Its distinct defect chemistry and the ability to exchange lattice oxygen with the gas phase results in an oxide with unique catalytic properties [32], including the promotion of metal dispersion, enhancement of the catalytic activity at the metal–support interface sites, and promotion of CO removal through oxidation using lattice oxygen. Earlier studies found that Au/ceria catalysts are very promising for the PROX reaction [23,33–41]. These catalysts exhibited high activity and good selectivity in the temperature range of 323–393 K. The presence of both CO_2 and H_2O diminished CO conversion, especially in the lower-temperature region [35–37]; however, Au/ceria catalysts were quite stable with time on stream, in contrast with other gold catalysts, such as Au/Fe_2O_3 [9,42] and Au/TiO_2 [43], which lost a significant portion of their initial activity during the first hours of reaction. More recently, no drop in the activity or selectivity of Au/CeO_2 was noted under cyclic operation up to 423 K [33].

The present work reports the results of a detailed study of the catalytic performance of gold supported on doped ceria in the PROX reaction. The ceria support was modified by the addition of various cations (i.e., Sm^{3+}, La^{3+}, and Zn^{2+}). The dopants were selected based on the findings of a recent study [44]. The dopant cations with ionic radius and electronegativity close to those of cerium cation are considered the most appropriate modifiers of structural and chemical properties of ceria. This is related to the heterocations' ability to cause structural distortions inside ceria, causing strain on the oxide lattice and favoring formation of oxygen vacancies. The aim of the present study was to obtain a defective fluorite structure with increased oxygen mobility that could result in enhanced activity and improved resistance toward deactivation caused by the presence of CO_2 and H_2O in the PROX feed. High-resolution transmission electron microscopy (HRTEM) measurements were combined with IR spectra of CO adsorption after different pretreatments and in $CO–O_2$, $CO–O_2–H_2$, and $CO–O_2–H_2–H_2O$ reaction mixtures, to correlate the dispersion and oxidation state of gold with the catalytic properties.

2. Experimental

2.1. Catalyst preparation

Doped ceria supports were synthesized by a coprecipitation method. Mixed aqueous solutions of nitrate salts of cerium and metal modifier at an atomic ratio of $M/(M + Ce) = 0.05$ (M: Sm, Zn, or La) and a precipitating agent, K_2CO_3, were added dropwise in a Contalab reactor while a constant pH of 9.0 and temperature of 333 K were maintained. The precipitates were aged for 1 h at 333 K, filtered, washed carefully until no NO_3^- ions were present, dried under vacuum at 353 K, and calcined in air at 673 K for 2 h. The same procedure was followed to prepare pure ceria. Gold was dispersed on the supports by deposition–precipitation. Gold hydroxide was deposited onto the support through a chemical interaction between $HAuCl_4{\cdot}3H_2O$ (Merck) and K_2CO_3 under vigorous stirring at constant pH of 7.0 and temperature of 333 K. After 1 h of aging, the precipitates were washed, dried in vacuum at 353 K, and calcined in air at 673 K for 2 h. The gold loading for each catalyst was 3 wt%.

2.2. Catalyst characterization

The specific surface areas of the catalysts, S_{BET}, were determined from the adsorption isotherms of nitrogen at 77 K using a Quantachrome Autosorb-1 instrument and following the BET (Brunauer–Emmett–Teller) procedure with six relative pressures of nitrogen in the range of 0.05–0.3. The crystalline structure of the catalysts was analyzed with a X-ray powder diffractometer (Bruker D8 Advance) using CuK_α radiation ($\lambda = 0.15418$ nm). The measurement was carried out in the 2θ angle range of 20°–80°.

The HRTEM analysis was performed using a Jeol JEM 2010 (200 kV) microscope equipped with an EDS Oxford Link analytical system. The powdered sample was ultrasonically dispersed in isopropyl alcohol, and the suspension thus obtained was deposited on a copper grid coated with a porous carbon film.

Temperature-programmed reduction (TPR) experiments were performed in a typical flow system [10], equipped with a mass spectrometer (Omnistar/Pfeiffer Vacuum) under a flow of a 3% H_2/He mixture (50 $cm^3\,min^{-1}$) over 50 mg of catalyst at a heating rate of 10 $K\,min^{-1}$. Each sample was pretreated at 673 K for 30 min under air flow before TPR.

The FTIR spectra were collected on a Perkin–Elmer 1760 spectrometer (equipped with a MCT detector) with the samples in self-supporting pellets introduced in a cell, to allow thermal treatment in a controlled atmosphere and spectrum scanning at a controlled temperature (from 90 K up to room temperature). Band integration was performed using Curvefit in Spectra Calc (Galactic Industries Co.) by means of Lorentzian curves. The spectrum of the sample before the CO inlet was subtracted from each spectrum.

2.3. Catalytic activity and selectivity

Activity and selectivity measurements for the PROX process were carried out at atmospheric pressure in a conventional fixed-bed reactor system, as described previously [10]. Before all catalytic measurements, the samples were treated in a flowing 20 vol% O_2/He mixture at 673 K for 30 min or a flowing 10 vol% H_2/He mixture at 373 K for 1 h, followed by cooling to the reaction temperature in pure He. The catalyst weight was 50–120 mg, and the total flow rate of the reaction mixture was 50–100 $cm^3\,min^{-1}$, yielding W/F ratios in the range of 0.03–0.144 $g\,s\,cm^{-3}$. The feed contained 1% CO, 1.25% O_2, 50% H_2, and the balance He. The effect of CO_2 was investigated after the addition of 15% CO_2 in the feed. To evaluate the effect of water vapor on the reaction, 10% H_2O was added to the dry gas stream through a syringe pump. The

gas lines were heated to 393 K to avoid water condensation before the reactor inlet. CO oxidation rates were measured under differential conditions, with CO conversion <10–15%. The catalyst was in the form of a powder with particle size of $90 < d_p < 180$ μm and mass of 10 mg, diluted at a 5:1 ratio with inert sea sand. Product and reactant analyses were carried out in a Shimadzu GC-14B gas chromatograph equipped with a thermal conductivity detector. The CO conversion calculation was based on the CO_2 formation or CO consumption (when an excess of CO_2 was added). The selectivity toward CO_2 production was calculated from the oxygen mass balance.

3. Results and discussion

3.1. PROX measurements

Fig. 1A shows the CO conversion and the selectivity toward CO_2 production of doped and undoped preoxidized Au/ceria catalysts. A positive effect of doping was found for the Zn^{2+} and Sm^{3+} dopants, whereas doping with La^{3+} decreased the catalytic activity. Thus, the following activity order was observed in the PROX reaction: Au/Zn–CeO_2 > Au/Sm–CeO_2 > Au/CeO_2 > Au/La–CeO_2. Under standard experimental conditions ($W/F = 0.03$ g s cm^{-3}), at 363 K, the maximum CO conversion achieved over the Zn-doped catalyst was 96% (with 40% selectivity), and that over the undoped catalyst was 88% (with 37% selectivity).

A reductive pretreatment at 373 K for 1 h enhanced the catalytic activity of all catalysts, as shown in Fig. 1B. The trend is the same as that over preoxidized catalysts. Arrhenius plots of CO oxidation over all catalysts, both preoxidized and prereduced, are shown in Fig. 2. The Zn- and Sm-doped Au/ceria catalysts still were more active than undoped Au/ceria, whereas the La-doped sample was slightly less active. The apparent activation energies of CO oxidation over the preoxidized samples were 31–41 kJ mol^{-1}, similar to those for the prereduced samples (29–38 kJ mol^{-1}).

Fig. 3 illustrates the effect of pretreatment on the catalytic performance of the most active catalyst, the Zn-doped catalyst. As shown, 98.2% CO conversion was obtained over the prereduced sample at 338 K with 47% selectivity, whereas 96% maximum CO conversion was obtained over the preoxidized sample at 363 K with 40% selectivity. The results of Jain et al. [39] also indicate that reduction of the Au/$CeLaO_x$ mixed oxide catalysts is important for high PROX activity.

A possible explanation of the promoting effect is that reaction of hydrogen with oxygen adsorbed on the gold clusters and oxygen species on the ceria surface in close contact with gold facilitates the formation of oxygen vacancy defects on ceria. Because the active sites are located at the metal–support interface perimeter [13–20], the presence of oxygen vacancies close to gold clusters plays an important role in the high catalytic activity. Very recent DFT calculations of Shapovalov et al. [45] and transient pulse titration measurements in a TAP reactor reported by Widmann et al. [46] clearly demonstrate the role of surface vacancies in activation of CO oxidation on ceria-supported Au catalysts. In addition, previous FTIR measurements on closely related samples (i.e., Au/CeO_2 catalysts prepared by deposition–precipitation and urea gelation/coprecipitation methods) revealed that in an oxidizing atmosphere, the electronic and structural features of gold supported on modified ceria differed from those in a reducing atmosphere, where the clusters are negatively charged and possibly flattened on the surface of the reduced support [47]. We present a detailed FTIR analysis later in the article.

As shown in Figs. 1 and 3, catalyst selectivity decreased with increasing temperature, reaching 35–45% at 343–363 K, where maximum CO conversion was seen (i.e., ~85–95%). In addition, a peak

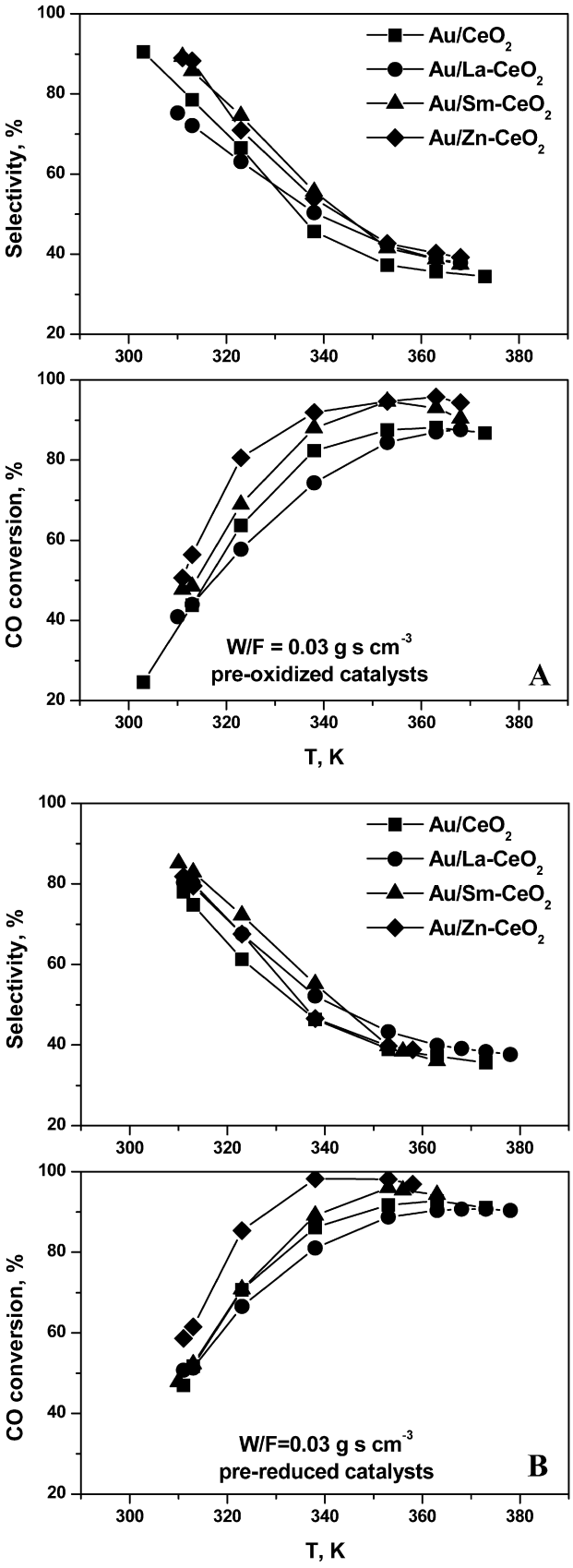

Fig. 1. Activity and selectivity towards CO_2 production of preoxidized (A) and prereduced (B) Au/CeO_2 (■), Au/Sm–CeO_2 (▲), Au/La–CeO_2 (●) and Au/Zn–CeO_2 (◆) catalysts for the PROX reaction at $W/F = 0.03$ g s cm^{-3}. Feed: 1% CO, 1.25% O_2, 50% H_2, He.

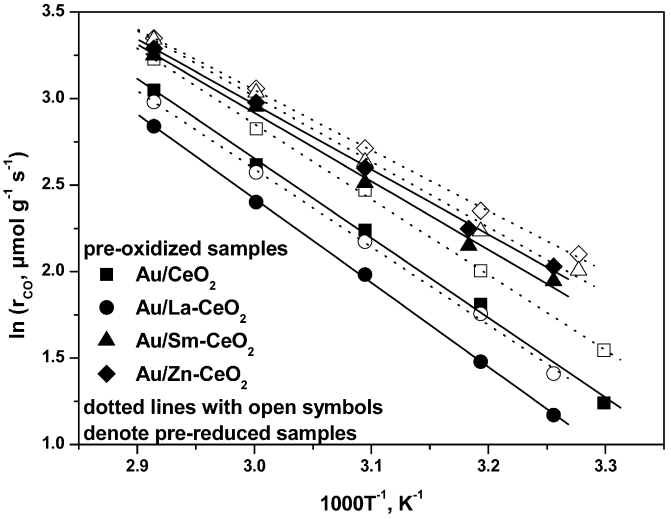

Fig. 2. Arrhenius plots of CO oxidation rates of preoxidized (solid symbols and lines) and prereduced (open symbols, dotted lines) Au/CeO_2 (■), $Au/Sm–CeO_2$ (▲), $Au/La–CeO_2$ (●) and $Au/Zn–CeO_2$ (◆) catalysts at $W/F = 0.03\ g\,s\,cm^{-3}$. Feed: 1% CO, 1.25% O_2, 50% H_2, He.

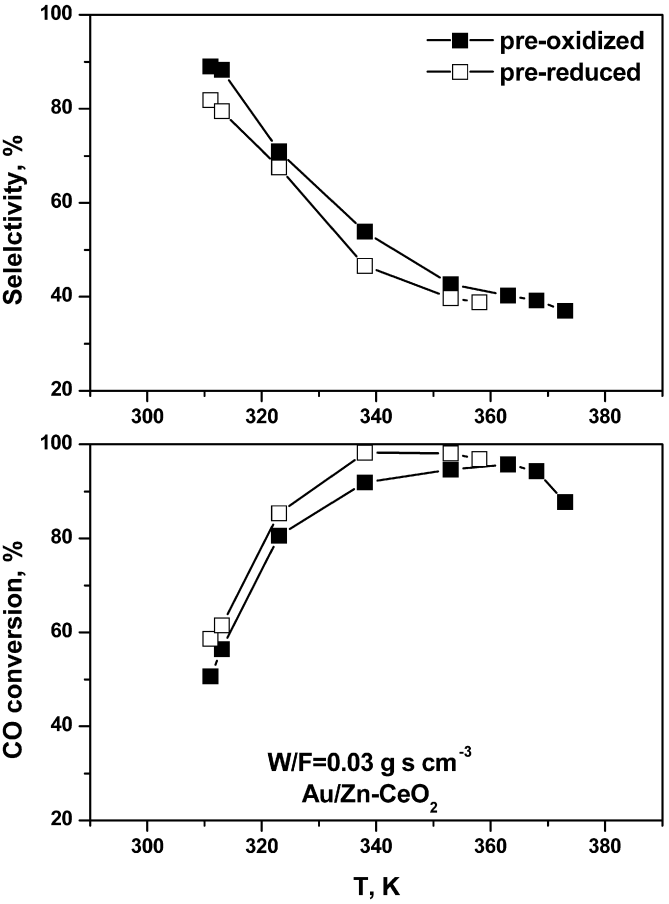

Fig. 3. Effect of a reducing (3% H_2/He, 1 h) pretreatment at 373 K (open symbols) on the activity and selectivity towards CO_2 of a preoxidized $Au/Zn–CeO_2$ catalyst for the PROX reaction at $W/F = 0.03\ g\,s\,cm^{-3}$. Feed: 1% CO, 1.25% O_2, 50% H_2, He.

was observed in all of the CO conversion curves, implying competitive consumption of oxygen by hydrogen with increasing temperature. Because the selectivity toward CO_2 production could be improved by lowering the operation temperature, the activity and selectivity of the samples also were evaluated at a higher W/F ratio of $0.144\ g\,s\,cm^{-3}$. The results, shown in Fig. 4, show that under

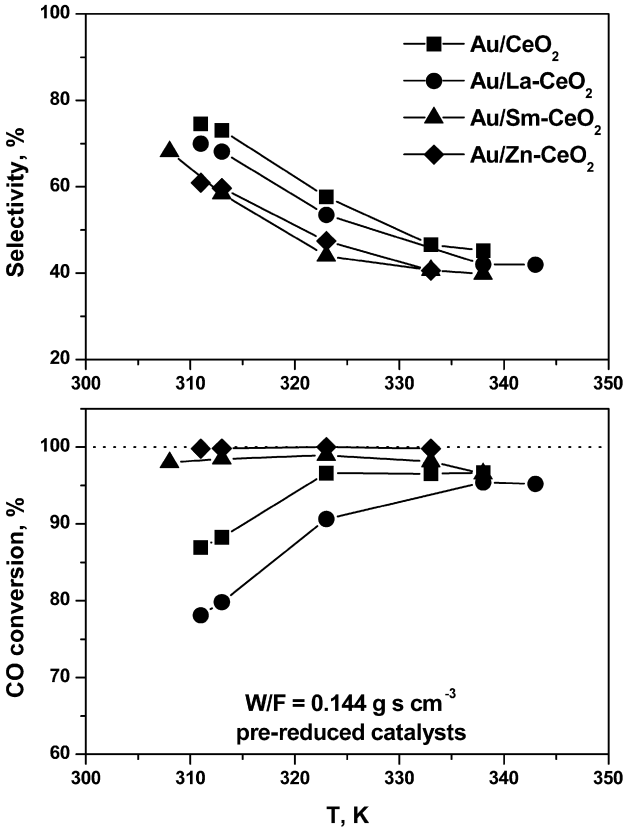

Fig. 4. Activity and selectivity towards CO_2 production of prereduced Au/CeO_2 (■), $Au/Sm–CeO_2$ (▲), $Au/La–CeO_2$ (●) and $Au/Zn–CeO_2$ (◆) catalysts for the PROX reaction at $W/F = 0.144\ g\,s\,cm^{-3}$. Feed: 1% CO, 1.25% O_2, 50% H_2, He.

these conditions, the catalysts exhibited remarkable performance in preferential CO oxidation, whereas the trends of activity and selectivity as functions of dopant type remained the same. Thus, the most active catalyst (i.e., the Zn-doped catalyst) attained 99.9% CO conversion (10 ppm residual CO) with 60% selectivity at 313 K, whereas the maximum CO conversion obtained over the undoped catalyst was 96.6% with 58% selectivity at 323 K. In contrast, the La-doped sample was the least active, exhibiting a maximum CO conversion of 95.4% with 42% selectivity at 338 K.

Fig. 5 illustrates the effect of the presence of 15% CO_2 in the reaction mixture on the catalytic performance of the various catalysts. As shown, the presence of CO_2 provoked a significant decrease in the activity of undoped Au/CeO_2 catalyst (Fig. 5A); maximum CO conversion (ca. 70%) was obtained at 353 K with 31% selectivity, compared with 96.6% at 323 K with 58% selectivity in the absence of CO_2 in the feed. Along with this negative effect on activity, the presence of CO_2 also diminished the selectivity. Indeed, a given CO conversion achieved in the absence of CO_2 was obtained less selectively in the presence of CO_2. But this effect was much more pronounced for the undoped sample, because doping had a beneficial effect on the catalyst's CO_2 tolerance. The Zn- and Sm-doped catalysts were found to be the most resistant toward deactivation by CO_2 (Figs. 5B and 5C), whereas the La-doped catalyst was the most sensitive (Fig. 5D) among the doped catalysts. The latter sample outperformed the undoped catalyst, in contrast to their behavior in the absence of CO_2 in the feed (Figs. 5A and 5D).

In contrast to the negative effect of CO_2 on activity and selectivity, coadding 10% H_2O in the reactant feed had a beneficial effect (Fig. 5). The presence of water improved the catalytic performance; this effect was more pronounced for the doped catalysts (Figs. 5B, 5C, and 5D). In the presence of both CO_2 and H_2O in the feed, the maximum CO conversion achieved was 78% at 348 K

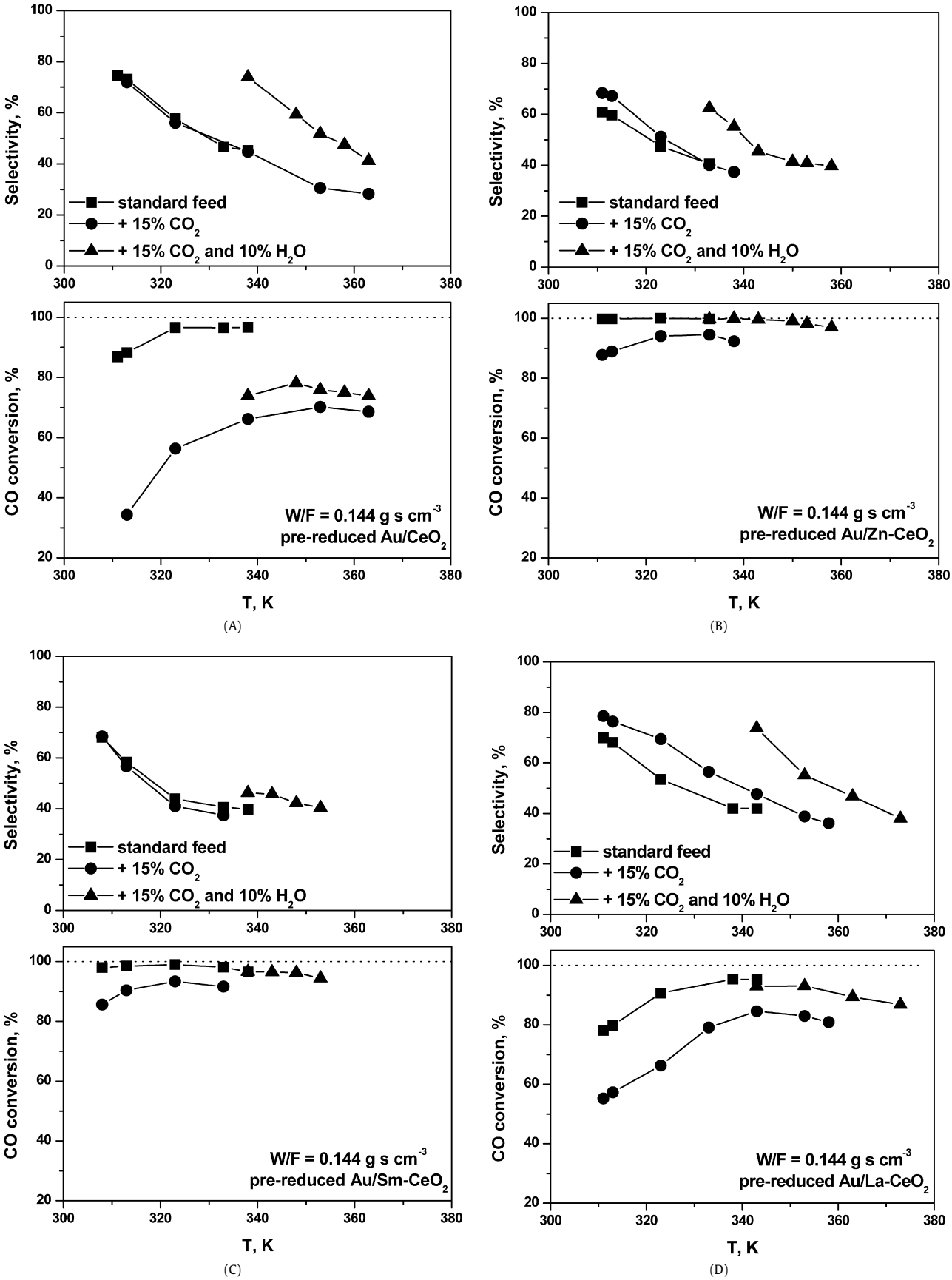

Fig. 5. Effect of CO_2 and H_2O addition on the activity and selectivity towards CO_2 production of prereduced (A) Au/CeO_2, (B) $Au/Zn–CeO_2$, (C) $Au/Sm–CeO_2$ and (D) $Au/La–CeO_2$ catalysts for the PROX reaction at $W/F = 0.144\ g\,s\,cm^{-3}$. Rectangles denote the standard feed: 1% CO, 1.25% O_2, 50% H_2, He. Circles denoted the presence of 15% CO_2 in the feed. Triangles denote the presence of both 15% CO_2 and 10% H_2O in the feed.

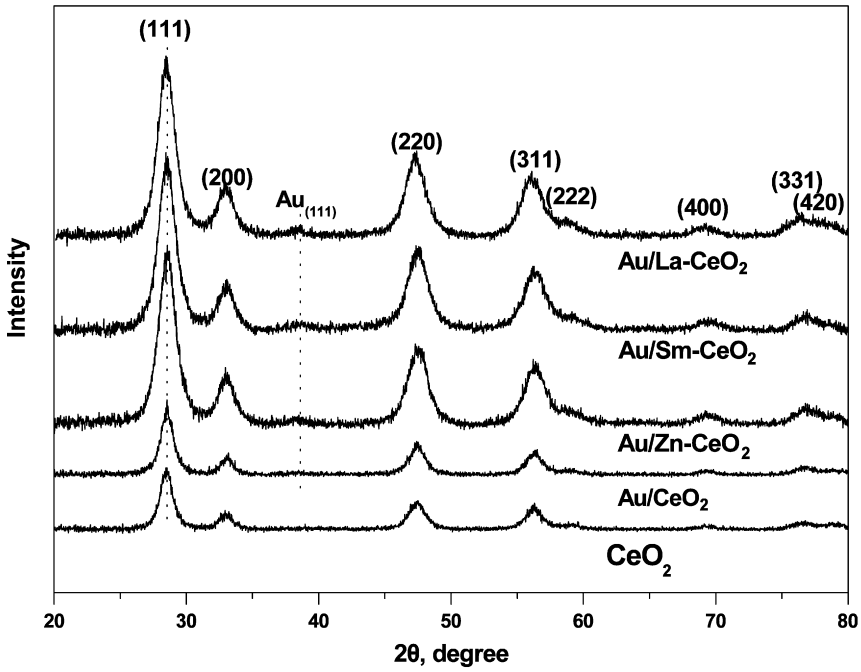

Fig. 6. XRD patterns of CeO_2, Au/CeO_2, $Au/La–CeO_2$, $Au/Sm–CeO_2$ and $Au/Zn–CeO_2$ catalysts.

(59% selectivity) for the undoped catalyst (Fig. 5A), 99.9% at 338 K (55% selectivity) for the Zn-doped catalyst (Fig. 5B), 96.6% at 338 K (46% selectivity) for the Sm-doped catalyst (Fig. 5C), and 93.1% at 353 K (55% selectivity) for the La-doped catalyst (Fig. 5D). As discussed previously [35–37], the negative effect of CO_2 is due to the competitive adsorption of CO (and H_2) and CO_2 on the catalyst surface. This was not the case when water was coadded in the feedstream, which improved both activity and selectivity. To elucidate this point, we performed FTIR characterization.

3.2. Catalyst characterization

3.2.1. BET, XRD, and HRTEM measurements

The modification of ceria with Sm^{3+}, La^{3+}, and Zn^{2+} cations led to a decrease in ceria's specific surface area. More specifically, the specific surface areas of the catalysts were 65 $m^2\,g^{-1}$ for Au/CeO_2, 63 $m^2\,g^{-1}$ for $Au/Zn–CeO_2$, 54 $m^2\,g^{-1}$ for $Au/Sm–CeO_2$, 53 $m^2\,g^{-1}$ for $Au/La–CeO_2$, and 70 $m^2\,g^{-1}$ for pure CeO_2.

The XRD patterns in Fig. 6 show the presence of the distinct fluorite-type oxide structure of CeO_2 in all samples. Observable shifts in the diffraction lines of CeO_2 were hardly seen in any of the catalysts; however, the XRD peaks of CeO_2 were broader in the doped samples, and shifts of small magnitude might as well have been undetectable. The XRD peak broadening and absence of cation oxide reflections suggest that part of the Sm^{3+}, La^{3+}, and Zn^{2+} cations were incorporated into the CeO_2 lattice, leading to formation of a solid solution. XPS studies of relevant materials (e.g., doped $CuO–CeO_2$) showed that samarium cations appeared to be fully incorporated into the ceria lattice, whereas most of the zinc oxide species were highly dispersed on the ceria surface [44]. The surface coverage of dopant cations increased with increasing cation concentration, indicating that most of the dopant species resided on the surface. Gold was highly dispersed on ceria, as indicated by the barely detectable corresponding XRD peaks of $Au_{(III)}$ in the doped catalysts, which implies the formation of gold particles <5 nm in size.

HRTEM measurements on Au/CeO_2 and on Au/doped samples are shown in Figs. 7 and 8. Significant differences have been observed among the samples even if a particle size distribution cannot be provided, due to the very difficult detection of gold on nanocrystalline ceria due to the low contrast [40,48]. A bimodal distribution of the gold, as demonstrated by the presence of both large gold particles at least 10 nm in size (indicated by white arrows in A) and very highly dispersed gold clusters with size of about 1 nm (B), whose composition is confirmed by EDS analysis, is evident on Au/CeO_2. For the doped catalysts, 3.5–4 nm gold particles have been found on the $Au/Sm–CeO_2$ sample (Fig. 8A). In contrast, no gold particles were detected on $Au/Zn–CeO_2$ (Fig. 8B), indicating higher gold dispersion than on $Au/Sm–CeO_2$, as we explore later in the discussion of the FTIR data (Section 3.2.3). As discussed by Sakurai et al. [49], very small Au nanoparticles could not be observed by conventional TEM, but could be detected by the ADF-STEM technique. Finally, gold particles of about 5 nm were present on the $Au/La–CeO_2$ catalyst (Fig. 8C). The HRTEM results are in good agreement with the XRD patterns (Fig. 6).

3.2.2. TPR measurements

H_2-TPR profiles of Au/doped-CeO_2 catalysts are presented in Fig. 9. A single peak is centered at ~396 K in the TPR profile of pure Au/ceria catalyst. The modification with cations of Sm and Zn causes a shift in the reduction temperature to lower values, 377 and 380 K, respectively, whereas in the presence of La^{3+}, the shift was in the opposite direction (peak maximum at 408 K). These differences in the TPR profiles possibly originated from the presence of dopants and/or from minor differences in the gold dispersion, as evidenced in HRTEM analysis. Arena et al. also reported a relationship between the extent of hydrogen consumption during the TPR experiments and the dispersion of the Au precursor [40]. Comparing the hydrogen consumption of the samples shows that the greatest amount of hydrogen is needed for the reduction of Au/CeO_2. This result may be correlated with HRTEM data, revealing high amounts of very small gold clusters on the surface for this sample. It already has been reported that very small gold particles and clusters are able to adsorb oxygen during calcination in air [50]. Additional evidence of the discussed TPR behavior was provided by FTIR spectroscopic experiments. The FTIR spectra collected after CO adsorption at 90 K on the as-prepared doped catalysts (spectra not shown) included a broad feature with two components centered at 2121 and 2103 cm^{-1}, which can be at-

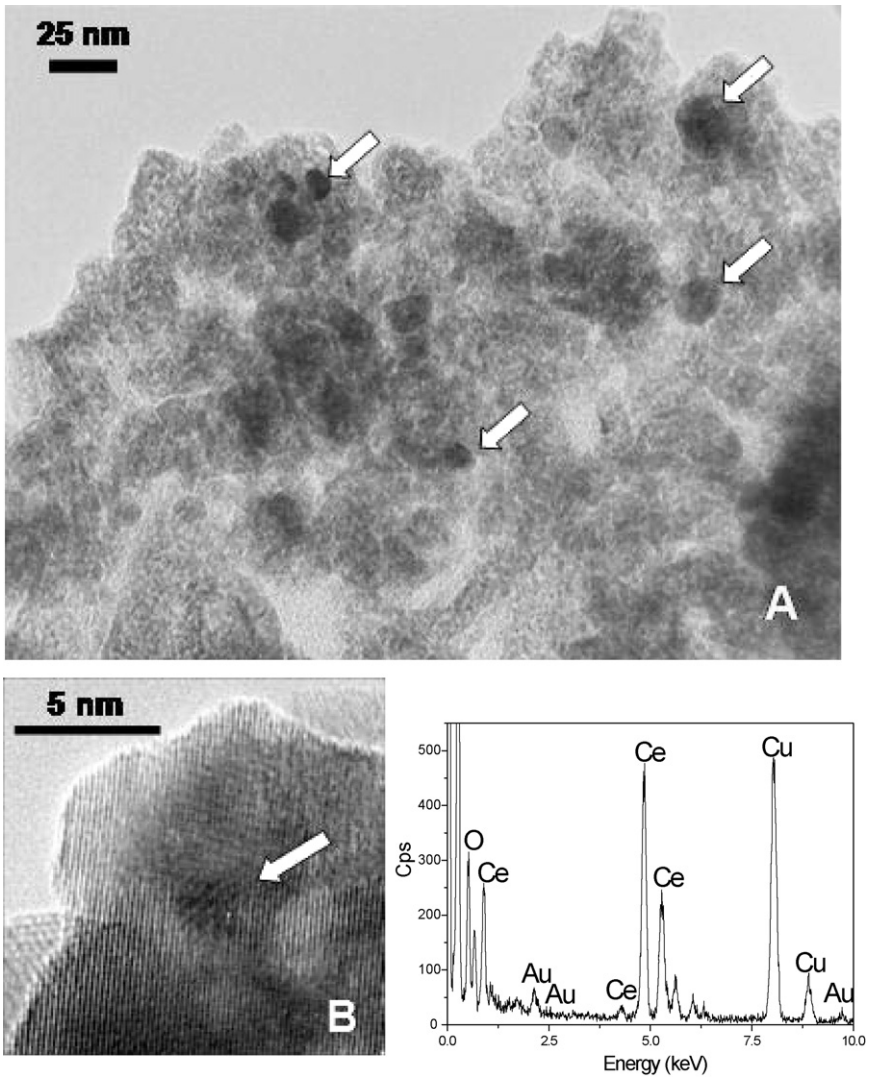

Fig. 7. TEM image of Au/CeO_2 (section A) and HRTEM of the same sample on which a detail showing a gold cluster (section B), whose EDS spectrum is also reported, are shown. Original magnification ×120 and ×800K, respectively.

tributed to the interaction of CO with $Au^{\delta+}$ and Au^0, respectively. In contrast, only a weak shoulder was registered in the same spectroscopic range in the spectrum of Au/CeO_2, because small gold particles ($d \leqslant 1$ nm) and clusters were covered by oxygen species. Thus, the hydrogen consumption could be attributed to the reduction of (i) oxygen adsorbed on very small gold particles and (ii) the surface oxygen of ceria located around the gold nanoparticles, which is strongly affected by them. The reduction process of modified with Sm and Zn ions Au/CeO_2 catalysts started at about 333 K, demonstrating the role of dopants in increasing the mobility of oxygen. Note that the TPR results correlate with the observed catalytic activity-selectivity trends in the PROX reaction.

3.2.3. Gold dispersion determined by FTIR CO absorption spectra

3.2.3.1. Calcined samples As described in Section 2, before the PROX catalytic tests, the samples were heated in a flowing 20 vol% O_2/He mixture at 673 K. Fig. 10A shows the FTIR spectra collected after CO adsorption at 90 K on the catalysts previously subjected to oxidation at 673 K and subsequent evacuation. The CO adsorption led to the appearance of an absorption band centered at 2101 cm^{-1} in the spectra of $Au/Zn–CeO_2$ (fine curve) and $Au/Sm–CeO_2$ (bold curve) catalysts, whereas a weak band at 2104 cm^{-1} was detected in that of Au/CeO_2 (dashed curve). These bands are assigned to CO adsorption on Au^0 step sites of gold nanoparticles [51]. Their intensity order of $Au/Sm–CeO_2(2.9) > Au/Zn–CeO_2(2.08) > Au/CeO_2(0.67)$ demonstrates a varying abundance of these sites on the samples. In particular, the relative intensities of these bands are in agreement with the HRTEM findings indicating a larger number of ≈3.5–4 nm gold particles on the $Au/Sm–CeO_2$ sample (Fig. 8A) and of ⩾10 nm gold particles along with highly dispersed clusters of about 1 nm on the Au/CeO_2 sample (Fig. 7). The very weak absorption in the region corresponding to CO on gold sites for Au/CeO_2 can be explained by taking into account that the large particles expose only a minimal number of step sites (i.e., only those sites able to adsorb CO), whereas small gold clusters ($d \leqslant 1$–2 nm) are covered by adsorbed oxygen after the calcination pretreatment [47,51–53].

3.2.3.2. Reduced samples CO adsorption on the reduced samples is of particular interest, because the PROX activity tests reported in Figs. 1–3 showed that a reductive pretreatment promoted catalytic activity. The adsorption of CO at 90 K on the undoped reduced catalyst (not shown) produced a large, intense absorption that was red-shifted at 2065 cm^{-1} with respect to the band position for metallic Au sites due to an electronic transfer from the reduced support to gold. This band has been assigned to CO on negatively charged gold clusters, as reported previously [52]. Moreover, as detected by HRTEM, only large metal particles and very small clusters

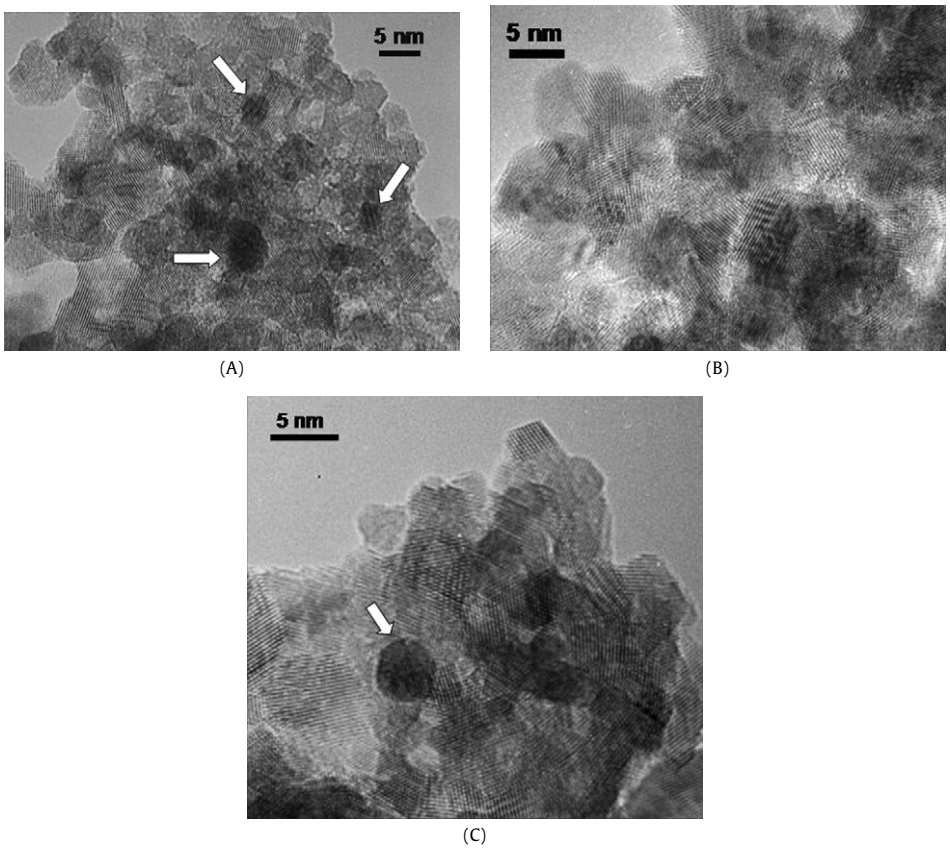

Fig. 8. HRTEM images of (A) Au/Sm–CeO_2, (B) Au/Zn–CeO_2 and (C) Au/La–CeO_2 catalysts. Original magnification ×800K.

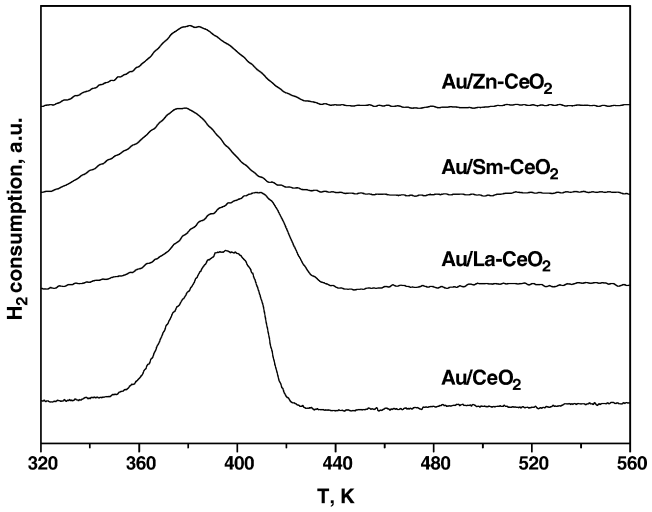

Fig. 9. H_2-TPR profiles of Au/CeO_2, Au/La–CeO_2, Au/Sm–CeO_2 and Au/Zn–CeO_2 catalysts.

were present on this sample, with no evidence of small (2–4 nm) particles and with a high concentration of step sites.

Fig. 10B compares the spectra of CO adsorbed at 90 K on Au/Zn–CeO_2 reduced at 373 K (fine curve) and at 423 K (bold curve). A reduction temperature of 423 K was chosen to simulate the experimental conditions during reduction before the PROX reaction. Keep in mind that the FTIR experiments were performed under static conditions, in which water produced in the reduction reaction may remain adsorbed to some extent, whereas the catalytic tests were performed under flowing conditions, facilitating water removal. The higher temperature can compensate for the lack of exchange between the reactant molecules seen under dynamic conditions. A broad band with a maximum at 2095 cm^{-1}, slightly red-shifted with respect to the usual position on other supported gold catalysts with a shoulder at about 2069 cm^{-1}, was present on the sample reduced at 373 K (fine curve). In agreement with previous results, these bands can be assigned to CO adsorbed on gold sites of small particles and to CO on clusters [51–53], respectively. A marked evolution of the band related to CO on gold sites occurred after reduction at 423 K (bold curve). The absorption band exhibiting a maximum at 2095 cm^{-1} after reduction at 373 K was shifted down to 2084 cm^{-1}, and a new component at 2018 cm^{-1}, indicative of electron-rich gold sites, was produced. The different charge of the dopant (Zn^{2+}) may have led to greater reducibility of the oxide and the possible formation of $AuCe_x$ clusters. At the same time, an increase in the integrated area normalized to the gold content of each pellet could be seen, starting from 2.39 on the sample reduced at 373 K and extending up to 4.36 on the sample reduced at 423 K. This behavior was not observed on any of the other doped samples, such as Au/Sm–CeO_2 (Fig. 10C). In this case, the increased reduction temperature produced no change in the position, shape, or intensity of the band, and the obtained integrated area remained almost constant (3.6). The results for the samples reduced at 423 K suggest a correlation between PROX activity and the integrated intensities of the CO absorption bands.

3.2.3.3. CO–O_2 interaction An IR experiment was performed to explore the role of dopants on the activity of the modified Au/CeO_2 catalysts. O_2 was admitted at 90 K on CO preadsorbed at the same temperature on the catalysts reduced previously at 373 K. Significant changes in the spectra were observed after 20 min of CO–O_2 interaction (Fig. 11A). Starting from the CO on reduced Au/CeO_2 as a reference (curve a), a weak absorption related to molecular

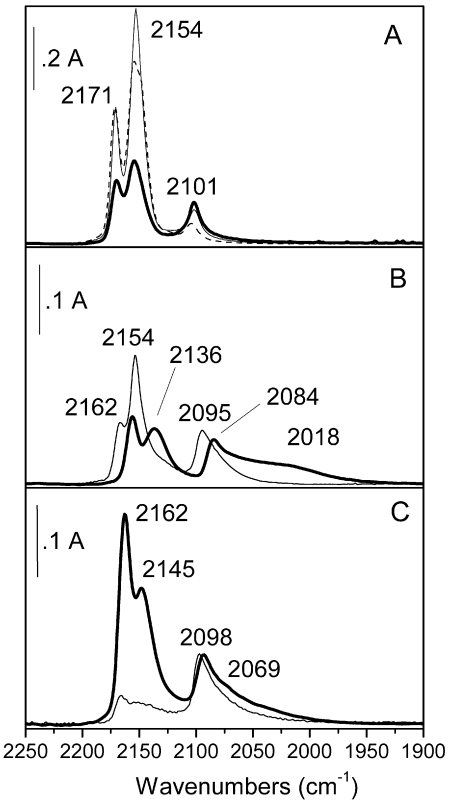

Fig. 10. Comparison of FTIR spectra in the carbonylic region of Au/CeO_2 (dashed curve), $Au/Zn–CeO_2$ (fine) curve) and $Au/Sm–CeO_2$ (bold curve) catalysts in contact with 0.5 mbar CO at 90 K; after oxidation treatment at 673 K (section A). Comparison between the spectra of $Au/Zn–CeO_2$ (section B) and of $Au/Sm–CeO_2$ (section C) after reduction at 373 (fine curves) and 423 K (bold curves). The spectra are normalized with respect to the gold content of each sample.

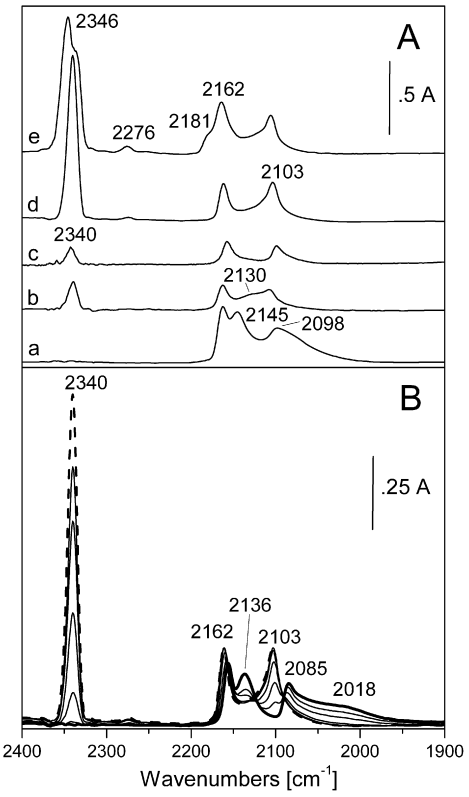

Fig. 11. Section A: FTIR absorption spectra after 20 min of interaction between O_2 admission at 90 K on 0.5 mbar of preadsorbed CO on the reduced catalysts (spectrum of Au/CeO_2 reported as reference, curve a): Au/CeO_2 (curve b), $Au/La–CeO_2$ (curve c), $Au/Zn–CeO_2$ (curve d), $Au/Sm–CeO_2$ (curve e). Section B: Evolution of FTIR absorbance spectra at 90 K after the inlet of O_2 on preadsorbed CO on $Au/Zn–CeO_2$ reduced at 423 K (bold curve); after 20 min (dashed curve). All spectra are normalized to the weight of the pellet.

CO_2 (i.e., a band at 2340 cm^{-1}) was noted after 20 min of $CO–O_2$ interaction (curve b), and the broad absorption related to CO adsorbed on small clusters was depleted, as was the band assigned to CO adsorbed on Ce^{3+} sites. Moreover, two components at 2103–2130 cm^{-1}, related to CO on mildly oxidized gold, were observed. As for the doped samples (curves c–e), greater amounts of CO_2 were produced in the presence of a high concentration of metallic gold particles on the surface of some of modified Au catalysts (curves d and e), as indicated by the higher intensity of the band at 2103 cm^{-1}, confirming the important role of metallic gold in the CO oxidation reaction. In addition, the lowest intensity of the same band, related to CO adsorption on metallic gold particles on the surface of $Au/La–CeO_2$, agreed closely with the catalytic performance of this sample. At the same time, bands at 1134 and at 840 cm^{-1}, assigned to superoxo species O_2^- and to peroxo O_2^- species adsorbed on reduced support sites [54], increased (spectra not shown). Evaluating the intensity of these bands after 20 min of reaction at 90 K reveals that the greatest abundance occurred on the surface of $Au/Sm–CeO_2$, whereas the lowest was found on $Au/La–CeO_2$. These species are related to the reduced sites at the interface with gold particles. Bands related to carbonate-like species also appeared on the surface of all catalysts in the 1800–800 cm^{-1} range.

Fig. 11 illustrates the evolution of the bands during a 20-min $CO–O_2$ interaction for the $Au/Zn–CeO_2$ sample (the most active one) after reduction at 423 K. The admission of O_2 at 90 K on preadsorbed CO (bold curve) resulted in strong erosion from the low-frequency side of the carbonylic band. In particular, the component at 2018 cm^{-1} was totally depleted, and conversion of the band at 2085 cm^{-1} to the band at 2103 cm^{-1} (i.e., the usual position of CO adsorbed on Au^0 sites) occurred, as indicated by the presence of an isosbestic point at 2090 cm^{-1}. Along with other changes at higher frequencies related to carbonylic species on the support, an intense band at 2340 cm^{-1}, due to the produced CO_2, was seen. This band also was observed during similar experiments performed in the presence of $^{18}O_2$ together with other components at 2323 cm^{-1} at 2305 cm^{-1}, assigned to the $C^{16}O^{18}O$ and $C^{18}O_2$ solid-like phases, respectively (data not shown). These species were completely absent in similar experiments performed at the same temperature on a Au/TiO_2 catalyst prepared by the deposition–precipitation method [51] and appear to be related to the very high oxygen mobility and exchange properties of ceria supports. The high intensity of the band ascribed to $C^{16}O^{18}O$ indicates that the oxygen participating in the reaction at 90 K originated mainly from the gas phase. This may suggest that oxygen molecules were somehow activated and dissociated on the sites at which CO was reversibly adsorbed at 90 K. Some of the atomic oxygen produced may react with CO, giving rise to the formation of $C^{16}O^{18}O$. Other oxygen atoms may remain coadsorbed with CO on the step sites, producing the component that was blue-shifted at 2120-cm^{-1}.

3.2.3.4. PROX and CO adsorption after reaction The PROX reaction at 90 K was studied on $Au/Zn–CeO_2$. First, an excess of hydrogen was contacted with the sample. Then the cell was cooled at 90 K, and a mixture of CO and oxygen (1:1) was admitted at the same temperature. Comparing the spectra collected after a 20-min interaction of CO and oxygen at 90 K in a H_2-free atmosphere (Fig. 12, solid curve) and a H_2-rich atmosphere (dashed curve) shows a similar nature and relative intensity of the absorption bands in the car-

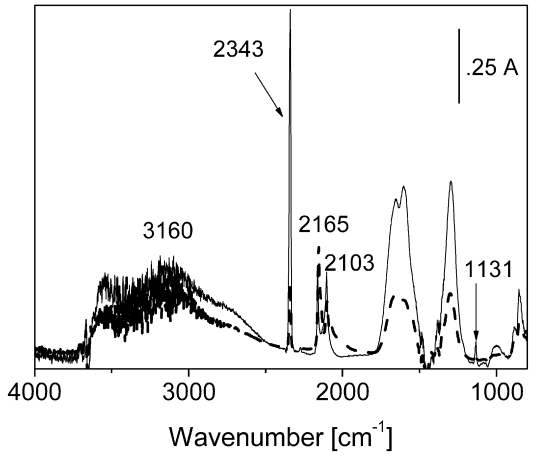

Fig. 12. Comparison between the FTIR spectra recorded after 20 min interaction at 90 K on Au/Zn–CeO_2 in: CO–O_2 (1:1) mixture—(solid curve); CO–O_2–H_2 (1:1:7) mixture—(dashed curve).

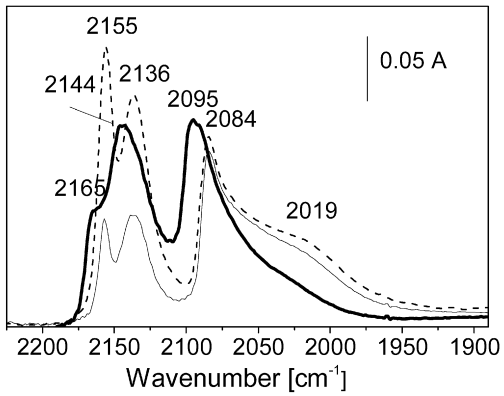

Fig. 13. FTIR absorbance spectra of Au/Zn–CeO_2 after CO (0.5 mbar) adsorption at 90 K on freshly reduced catalyst (dashed curve); after PROX at 400 K and outgassing (fine curve) and after PROX in the presence of water and outgassing (bold curve).

bonylic stretching region. In contrast, the species detected in the carbonate stretching region were less abundant in the presence of hydrogen than those detected in the CO–O_2 mixture. The positive effect of hydrogen could be related to the inhibited formation of stable carbonates in a similar way as was reported previously for the PROX reaction on Au/ZnO [55]. A pronounced effect of hydrogen on the CO oxidation rate on Au/TiO_2 also has been reported by Schumacher et al. [56]. These authors proposed that water (not added, but formed from reaction of hydrogen with oxygen) inhibited the formation of formate and carbonate species, accounting for the much lower tendency toward carbonate formation with water-induced conversion and decomposition of carbonate species.

The surface state of the most active catalyst (i.e., Au/Zn–CeO_2) after the PROX reaction at 400 K was studied by FTIR spectroscopy. In these experiments, Au/Zn–CeO_2 was contacted with the PROX mixture (CO–O_2–H_2 (1:1:7) with or without water and heated at 400 K for 20 min. Once the catalyst was cooled to room temperature, the spectra were collected (not shown). The most interesting results are those obtained by CO adsorption at 90 K after reaction at 400 K and outgassing. Examining the spectra in the 2200–1900 cm^{-1} range (Fig. 13) suggests that no agglomeration and/or deactivation by carbonates of highly dispersed gold species occurred either after the PROX reaction at 400 K or after the same reaction in the presence of water. In particular, the position, intensity, and shape of the band of CO adsorbed on gold species were practically the same after PROX (fine curve) as in the freshly reduced sample (dashed curve). As for the carbonyls on the support, their intensity decreased after PROX, due to the presence of carbonates partially covering the support surface sites.

When the PROX reaction was performed at 400 K in the presence of water, the CO adsorbed after reaction produced a blue-shifted band at 2096 cm^{-1} with a shoulder toward lower frequencies (bold curve). Moreover, the component at 2018 cm^{-1}, related to electron-rich Au sites (possibly Au–Ce alloy clusters), was totally depleted. At the same time, a new intense band at 2143 cm^{-1} and a weak component at 2162 cm^{-1} were produced. Specifically, this behavior is due to the presence of water, which reacts with the reduced support and the Au–Ce alloy, leading to O–H bond-breaking and formation of $Ce(OH)_x$ species [57]. Finally, comparing the integrated areas of the bands produced after CO adsorption at 90 K on Au sites on (i) freshly reduced Au/Zn–CeO_2 (dashed curve), (ii) the sample outgassed after PROX reaction (fine curve), and (iii) the sample outgassed after the PROX reaction in the presence of water (bold curve) showed very similar values. This indicates that almost all of the active gold sites detected before the PROX reaction were still available. These results correlate with the catalytic activity/selectivity tests demonstrating the ability of Au/doped-ceria catalysts to tolerate significant amounts of CO_2 and H_2O in the feed. Gold catalysts on modified ceria showed better activity and selectivity in the presence of both CO_2 and H_2O compared with undoped Au/CeO_2.

4. Conclusion

HRTEM and FTIR CO adsorption characterization have demonstrated that the dispersion of gold species formed on ceria doped with Sm^{3+}, La^{3+}, and Zn^{2+} cations was influenced by the dopant. Both large gold particles (>10 nm) and highly dispersed gold clusters (~1 nm) were found on Au/CeO_2 catalyst, whereas the gold particle size was ~5 nm for Au/La–CeO_2 and 3.5–4 nm for Au/Sm–CeO_2. The highest dispersion of gold was found on the Au/Zn–CeO_2 catalyst.

The activity order observed in the PROX reaction was Au/Zn–CeO_2 > Au/Sm–CeO_2 > Au/CeO_2 > Au/La–CeO_2. The intensity of the bands assigned to CO adsorbed on gold sites of the prereduced samples and during CO–O_2 interaction followed the same order.

The presence of excess CO_2 in the reactant feed provoked a decrease in the activity of all of the catalysts, especially the undoped one. Co-addition of CO_2 and H_2O had a beneficial effect on the catalytic performance of all of the samples, with the most pronounced effect seen for the doped samples.

Acknowledgments

J.P., G.A., and T.I. thank the Greek Ministry of Development, General Secretariat for Research and Technology for financial support in the framework of the Greece–Bulgaria bilateral S&T cooperation program. T.T. and V.I. gratefully acknowledge financial support from the Bulgarian Ministry of Education and Science, National Science Fund (project BG-7), and M.M. and F.B. gratefully acknowledge support from COFIN 2006.

References

[1] C. Song, Catal. Today 77 (2002) 17.
[2] A. Biyikoglu, Int. J. Hydrogen Energy 30 (2005) 1181.
[3] J. Papavasiliou, G. Avgouropoulos, T. Ioannides, Appl. Catal. B 66 (2006) 168.
[4] P.K. Cheekatamarla, C.M. Finnerty, J. Power Sources 160 (2006) 490.
[5] G.A. Olah, A. Goeppert, G.K.S. Prakash, Beyond Oil and Gas: The Methanol Economy, Wiley–VCH, 2006.
[6] B. Lindstrom, L.J. Pettersson, J. Power Sources 118 (2003) 71.
[7] G. Avgouropoulos, T. Ioannides, Appl. Catal. B 56 (2005) 77.
[8] Z. Qi, S. Buelte, J. Power Sources 161 (2006) 1126.

[9] G. Avgouropoulos, T. Ioannides, Ch. Papadopoulou, J. Batista, S. Hocevar, H. Matralis, Catal. Today 75 (2002) 157.
[10] G. Avgouropoulos, T. Ioannides, Appl. Catal. A 244 (2003) 155.
[11] G.J. Hutchings, J. Catal. 96 (1985) 292.
[12] M. Haruta, T. Kobayashi, H. Sano, N. Yamada, Chem. Lett. (1987) 405.
[13] M. Haruta, Catal. Today 36 (1996) 153.
[14] G.C. Bond, D.T. Thompson, Catal. Rev. Sci. Eng. 41 (1999) 319.
[15] M. Haruta, M. Date, Appl. Catal. A 222 (2001) 427.
[16] T.V. Choudhary, D.W. Goodman, Top. Catal. 21 (2002) 25.
[17] M. Haruta, Gold Bull. 37 (2004) 27.
[18] G.J. Hutchings, Gold Bull. 37 (2004) 3.
[19] G. Pattrick, E. van der Lingen, C.W. Corti, R.J. Holliday, D.T. Thompson, Top. Catal. 30 (2004) 273.
[20] G.C. Bond, C. Louis, D.T. Thompson, Catalysis by Gold, Catalytic Sci. Series, vol. 6, Imp. College Press, 2006.
[21] M. Haruta, S. Tsubota, T. Kobayashi, H. Kageyama, M. Genet, B. Delmon, J. Catal. 144 (1993) 175.
[22] M. Haruta, N. Yamada, T. Kobayashi, S. Iijima, J. Catal. 115 (1989) 301.
[23] M.M. Schubert, V. Plzak, J. Garche, R.J. Behm, Catal. Lett. 76 (2001) 143.
[24] M.M. Schubert, S. Hackenberg, A.C. van Veen, M. Muhler, V. Plzak, R.J. Behm, J. Catal. 197 (2001) 113.
[25] A. Luengnaruemitchai, D.T.K. Thoa, S. Osuwan, E. Gulari, Int. J. Hydrogen Energy 30 (2005) 981.
[26] C. Rossignol, S. Arrii, F. Morfin, L. Piccolo, V. Caps, J. Rousset, J. Catal. 230 (2005) 476.
[27] R.J.H. Grisel, B.E. Nieuwenhuys, J. Catal. 199 (2001) 48.
[28] R.H. Torres Sanchez, A. Ueda, K. Tanaka, M. Haruta, J. Catal. 168 (1997) 125.
[29] R.J.H. Grisel, C.J. Weststrate, A. Goossens, M.W.J. Craje, A.M. Van der Kraan, B.E. Nieuwenhuys, Catal. Today 72 (2002) 123.
[30] M.J. Lippits, A.C. Gluhoi, B.E. Nieuwenhuys, Top. Catal. 44 (2007) 159.
[31] C. Galletti, S. Fiorot, S. Specchia, G. Saracco, V. Specchia, Chem. Eng. J. 134 (2007) 45.
[32] A. Trovarelli, Catal. Rev. Sci. Eng. 38 (1996) 439.
[33] W. Deng, J. De Jesus, H. Saltsburg, M. Flytzani-Stephanopoulos, Appl. Catal. A 291 (2005) 126.
[34] L. Chang, N. Sasirekha, Y. Chen, W. Wang, Ind. Eng. Chem. Res. 45 (2006) 4927.
[35] G. Panzera, V. Modafferi, S. Candamano, A. Donato, F. Rusteri, P.L. Antonucci, J. Power Sources 135 (2004) 177.
[36] G. Avgouropoulos, J. Papavasiliou, T. Tabakova, V. Idakiev, T. Ioannides, Chem. Eng. J. 124 (2006) 41.
[37] A. Luengnaruemitchai, S. Osuwan, E. Gulari, Int. J. Hydrogen Energy 29 (2004) 429.
[38] O. Goerke, P. Pfeifer, K. Schubert, Appl. Catal. A 263 (2004) 11.
[39] A. Jain, X. Zhao, S. Kjergaard, S.M. Stagg-Williams, Catal. Lett. 104 (2005) 191.
[40] F. Arena, P. Famulari, G. Trunfio, G. Bonura, Appl. Catal. B 66 (2006) 81.
[41] E. Ko, E.D. Park, K.W. Seo, H.C. Lee, D. Lee, S. Kim, Catal. Today 116 (2006) 377.
[42] M.J. Kahlich, H.A. Gasteiger, R.J. Behm, J. Catal. 182 (1999) 430.
[43] S.D. Lin, M. Bollinger, M.A. Vannice, Catal. Lett. 17 (1993) 245.
[44] J. Papavasiliou, G. Avgouropoulos, T. Ioannides, Appl. Catal. B 69 (2006) 226.
[45] V. Shapovalov, H. Metiu, J. Catal. 245 (2007) 205.
[46] D. Widmann, R. Leppelt, R.J. Behm, J. Catal. 251 (2007) 437.
[47] M. Manzoli, F. Boccuzzi, A. Chiorino, F. Vindigni, W. Deng, M. Flytzani-Stephanopoulos, J. Catal. 245 (2007) 308.
[48] T. Akita, M. Okumura, K. Tanaka, M. Kohyama, M. Haruta, Catal. Today 117 (2006) 62–68.
[49] H. Sakurai, T. Akita, S. Tsubota, M. Kiuchi, M. Haruta, Appl. Catal. A 291 (2005) 179.
[50] V.A. Bondzie, S.C. Parker, C.T. Campbell, Catal. Lett. 63 (1999) 143.
[51] F. Boccuzzi, A. Chiorino, M. Manzoli, P. Lu, T. Akita, S. Ichikawa, M. Haruta, J. Catal. 202 (2001) 256.
[52] T. Tabakova, F. Boccuzzi, M. Manzoli, J.W. Sobczak, V. Idakiev, D. Andreeva, Appl. Catal. B 49 (2004) 73.
[53] F. Vindigni, M. Manzoli, A. Chiorino, T. Tabakova, F. Boccuzzi, J. Phys. Chem. B 110 (2006) 23329.
[54] V.V. Pushkarev, V.I. Kovalchuk, J.L. d'Itri, J. Phys. Chem. B 108 (2004) 5341.
[55] M. Manzoli, A. Chiorino, F. Boccuzzi, Appl. Catal. B 52 (2004) 259.
[56] B. Schumacher, Y. Denkwitz, V. Plzak, M. Kinne, R.J. Behm, J. Catal. 224 (2004) 449.
[57] X. Zhao, S. Ma, J. Hrbek, J.A. Rodriguez, Surf. Sci. 601 (2007) 2445.